

飞秒激光织构钛合金表面形貌及润湿性研究

肖蒲庐^{1,2}, 陈观华^{1,2}, 陈宇⁵, 张翔^{1,2,3,4}, 袁孝^{1,2,3,4*}¹苏州大学光电科学与工程学院, 江苏 苏州 215006;²苏州大学苏州纳米科技协同创新中心, 江苏 苏州 215006;³江苏省先进光学制造技术重点实验室, 江苏 苏州 215006;⁴苏州大学教育部现代光学技术重点实验室, 江苏 苏州 215006;⁵奥徒(上海)激光技术有限公司, 江苏 苏州 215123

摘要 通过改变飞秒激光的能量密度和扫描次数,分别采用 90°和 60°两种激光交叉线扫描方式,在钛合金表面制备了一系列方形和菱形微结构,系统地研究了飞秒激光参数对表面形貌和润湿性的影响。利用 X 射线光电子能谱测量分析了激光织构前后的表面化学成分变化。结果表明:表面结构的轮廓形貌更加依赖于激光的能量密度,而扫描次数主要影响结构的特征尺寸。不同的飞秒激光参数下获得的织构钛合金表面表现出不同程度的亲水性提升。较高的激光能量密度和扫描次数有利于增大钛合金表面的粗糙度,同时导致大量的金属氧化物富集,从而促进了液滴的浸润。

关键词 激光技术; 飞秒激光; 表面织构; 钛合金; 亲水性

中图分类号 TN249

文献标志码 A

DOI: 10.3788/CJL230431

1 引言

钛合金具有比重轻、耐腐蚀的特点,有着比其他植入材料更好的抗压强度和断裂韧性^[1],目前已成为牙科与骨科种植体领域的常用材料。但由于钛合金存在生物惰性,长期植入可能诱发种植体周围产生炎症^[2]并最终导致种植失败。大量研究证实:通过改变表面化学成分、粗糙度和表面自由能等表面特性,可以显著改善种植体材料与周围骨组织的结合水平,从而提高牙科与骨科种植体的生物相容性^[3-4]。润湿性作为影响种植体骨整合的重要因素,引起了越来越多的关注。与疏水表面相比,亲水表面能够促进早期蛋白质的吸附和随后的细胞黏附,在骨整合方面更具吸引力^[5]。

表面润湿改性一般是通过阳极氧化^[6]、等离子体刻蚀^[7]、化学蚀刻^[8]等传统加工技术来实现的。然而,这些加工技术制备出的表面结构大多分布随机,所涉及的程序步骤复杂且容易引入表面污染物^[9],存在一定的局限性。与传统加工技术相比,飞秒激光加工技术具有加工精度高、非接触和高灵活性等优势^[10-11],近年来已成为最具潜力的表面改性技术之一。基于激光束聚焦,能够以可控的方式将能量沉积在材料的表面,从而有效地实现预期设计结构的创建^[12]和润湿改性。Cunha 等^[13]利用波长为 1030 nm、脉冲宽度为 500 fs 的

飞秒激光,在 Ti6Al4V 表面上研究了四种类型结构的表面润湿行为,结果表明:激光处理后的表面都表现出亲水性以及对盐水溶液的高亲和力,表面纹理的各向异性导致了润湿行为的各向异性。Huerta-Murillo 等^[14]利用纳秒激光和飞秒激光在钛合金表面创建了微纳米双尺度结构,分析了在两种储存条件下织构表面的润湿行为。Schnell 等^[15]通过调控飞秒激光参数,在 Ti6Al4V 表面制备了不同尺度的微米和纳米结构,并研究了激光加工后第 1 天和第 7 天的表面润湿性。Pallarés-Aldeiturriaga 等^[16]使用不同波长的飞秒激光,在 Ti6Al4V 表面诱导了周期性纳米波纹结构,并研究了灭菌前后的表面润湿性。在众多的研究工作中,由于飞秒激光创建结构的多样性^[17-19],钛合金表面结构特征与润湿状态之间的关系至今尚未明确。为满足医疗植入工程的应用需求,研究不同飞秒激光参数下钛合金表面的润湿响应机制具有实际意义。

表面形貌一直是影响种植体与周围组织相互作用的重要因素。为进一步发挥天然骨骼内部结构的潜在优势,凹坑与沟槽这类地势结构^[20-21]所产生的生物学效应近年来已经被大量研究。网格状结构表面尽管研究较少,但其表现出的润湿性和生物功能作用在改善种植体的骨整合方面很有前途^[22-23]。因此,本文采用 90°和 60°两种激光交叉扫描策略,在钛合金表面开展

收稿日期: 2023-01-03; 修回日期: 2023-02-14; 录用日期: 2023-03-07; 网络首发日期: 2023-03-13

基金项目: 国家自然科学基金(61775153, U1930106)、江苏高校优势学科建设工程资助项目(PAPD)

通信作者: *xyuan@suda.edu.cn

了表面形貌和润湿性的实验研究。通过改变飞秒激光的能量密度和扫描次数,制备了一系列具有不同结构特征的方形和菱形结构表面。结合这些表面结构的截面轮廓和尺寸特征,系统地阐明了飞秒激光参数下钛合金表面结构形貌的演化规律。此外,测量了不同飞秒激光参数下钛合金表面的润湿性,并从表面形貌和表面化学成分两个角度分析了飞秒激光织构后钛合金表面润湿性的改变原因。

2 实验材料和方法

2.1 样品预处理

本实验使用的材料为医用五级 Ti6Al4V 合金,在激光加工前被切割制备成了尺寸为 10.0 mm × 10.0 mm × 0.5 mm 的方形薄板若干。先用砂磨轮搭配电磨机以 23000 r/min 转速进行打磨抛光,去除材料表面的杂质和有机污染物。然后将抛光后的样品放置在含有去离子水、无水乙醇、丙酮的混合液体中进行超声浴洗,总时长为 15 min。最后,使用无尘洁净布擦拭并自然干燥。

2.2 激光织构

飞秒激光加工系统原理图如图 1 所示。实验采用中心波长为 1030 nm、脉冲宽度为 300 fs 的掺镱光纤激光器进行表面织构处理,激光系统的脉冲重复频率可调节范围为 1 Hz~40 MHz。激光束经过 3 倍准直扩束,由反射镜反射进入扫描仪,再通过焦距为 100 mm 的远心镜聚焦到样品表面。实验中的聚焦光斑直径采用面积推算法^[24]推算为 25 μm,这与理论计算结果保持一致。利用计算机软件可以任意调节激光输出的平均功率,并通过控制运动平台实现样品选择性区域的精确对焦。

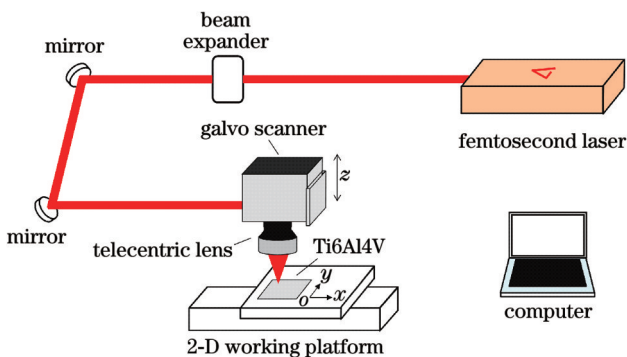


图 1 飞秒激光织构系统示意图

Fig. 1 Schematic of femtosecond laser texturing system

激光织构过程采用两种交叉线扫描路径策略,如图 2 所示,在 Ti6Al4V 合金表面的两个不同方向上依次进行逐行扫描。为了创建具有周期性分布的规则微结构表面,前期开展大量实验与形貌观测以获取合适的激光加工参数。最终,保持激光的扫描速度(v)为 300 mm/s,扫描线间距(Δd)固定为 25 μm。

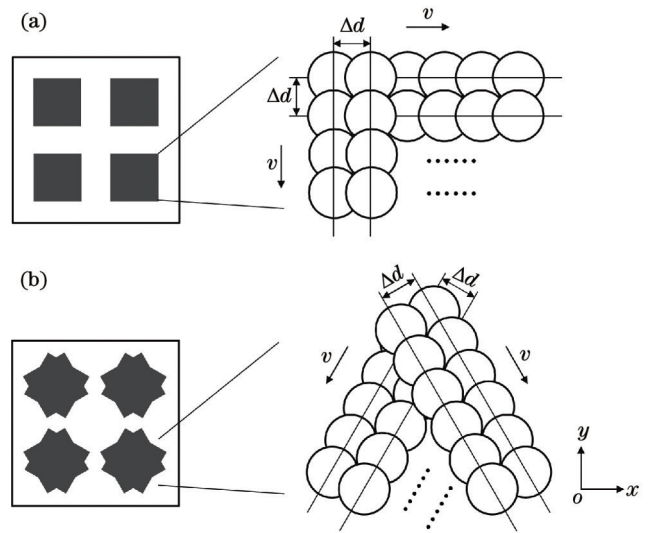


图 2 激光交叉线扫描路径策略示意图。(a)90°激光交叉线扫描;(b)60°激光交叉线扫描

Fig. 2 Schematics of laser cross-line scanning path strategy. (a) 90° laser cross-line scanning; (b) 60° laser cross-line scanning

本研究中,通过改变飞秒激光的能量密度(F)和扫描次数(N)织构了一系列具有不同结构特征的表面,具体的激光参数如表 1 所示。为了有效地讨论激光参数对表面结构和润湿性的影响,使用以上两种扫描路径策略制备了 16 个样品。在脉冲重复频率为 100 kHz 的条件下,通过改变激光功率来调控激光的能量密度 F 。所有样品的加工过程均在具有恒定温度和湿度的标准大气环境中进行。

表 1 飞秒激光加工参数

Table 1 Femtosecond laser processing parameters

Sample No.	$F / (J/cm^2)$	N
1	0.20	10
2	0.90	10
3	2.31	10
4	5.51	10
5	0.20	5
6	0.20	25
7	0.20	50
8	2.31	50

2.3 表面表征

在 10 kV 加速电压下,使用扫描电子显微镜 (SEM) 观察加工后样品表面的结构形貌。通过共聚焦显微镜测量激光织构后表面结构的截面轮廓和表面粗糙度(S_a),以获取表面结构的具体尺寸信息,测量时所用物镜的放大倍数为 100,测量面积为 175.31 μm × 131.97 μm。采用视频光学接触角测量仪测量样品表面的静态接触角,以评估表面的润湿性能,单次测量使

用的去离子水体积为 $1.5 \mu\text{L}$ 。每种织构表面重复测量三次,并计算测量结果的平均值和标准差。最后,利用 X 射线光电子能谱检测飞秒激光织构前后样品表面的化学成分变化。

3 分析与讨论

图 3 为飞秒激光织构后的钛合金表面 SEM 图像。在激光逐行扫描的交叉重叠区域获得了不同的表面结构形貌,这与激光能量密度和扫描次数的改变密切相关。其中,图 3(a1)~(a4)和图 3(b1)~(b4)分别显示了不同激光能量密度下表面结构形貌的演化过程。当激光能量密度 F 为 0.20 J/cm^2 时,强度呈高斯分布的激光束以非静态的加工方式完成扫描后,扫描路径上覆盖了一层激光诱导周期性波纹结构(LIPSS),如图 3(a1)、(b1)所示。LIPSS 通常出现在能量密度略高于烧蚀阈值并且存在入射激光脉冲辐照的情况下。目前普遍认为,这种结构的形成归因于入射线偏振光与被激发的表面等离子体激元之间的干涉^[25]。随着激光能量密度的增加,材料表面的烧蚀程度加剧,微米结构顶部开始出现凸起的现象,如图 3(a2)、(b2)所示。

高斯脉冲作用区域内强度分布的不一致引起了局部温差,导致表面张力发生改变^[26],进而使得烧蚀产生的熔融态物质在张力梯度的作用下向扫描路径两旁堆积,最终冷凝后形成了重铸层。此外,激光能量密度的进一步增加使得烧蚀羽流中的粒子增多,迅速冷却后沉积在钛合金表面,并最终形成了致密的纳米颗粒。当激光能量密度 F 增加到 5.51 J/cm^2 时,从图 3(a4)、(b4)可以清楚地观察到与流体力学相关的熔体痕迹。

与激光能量密度相比,扫描次数对表面结构形貌的影响存在差异。图 3(a5)~(a7)和图 3(b5)~(b7)分别显示了不同扫描次数下利用两种激光交叉线扫描方式织构获得的表面形貌。在加工过程中,由于激光始终保持较低的入射能量密度,表面的烧蚀行为一般表现为温和烧蚀,气化过程占据主导地位,暂不考虑熔化飞溅和相爆炸等强烈烧蚀过程。因此,激光扫描路径上的 LIPSS 并未随着扫描次数的增加而消失。同时,微结构单元的边缘在多次扫描后出现了重铸层,并在扫描路径的交叉处产生了孔洞和裂纹,但由于熔化形成的重铸层较少,微结构单元的顶部并未完全被覆盖,如图 3(a7)、(b7)所示。

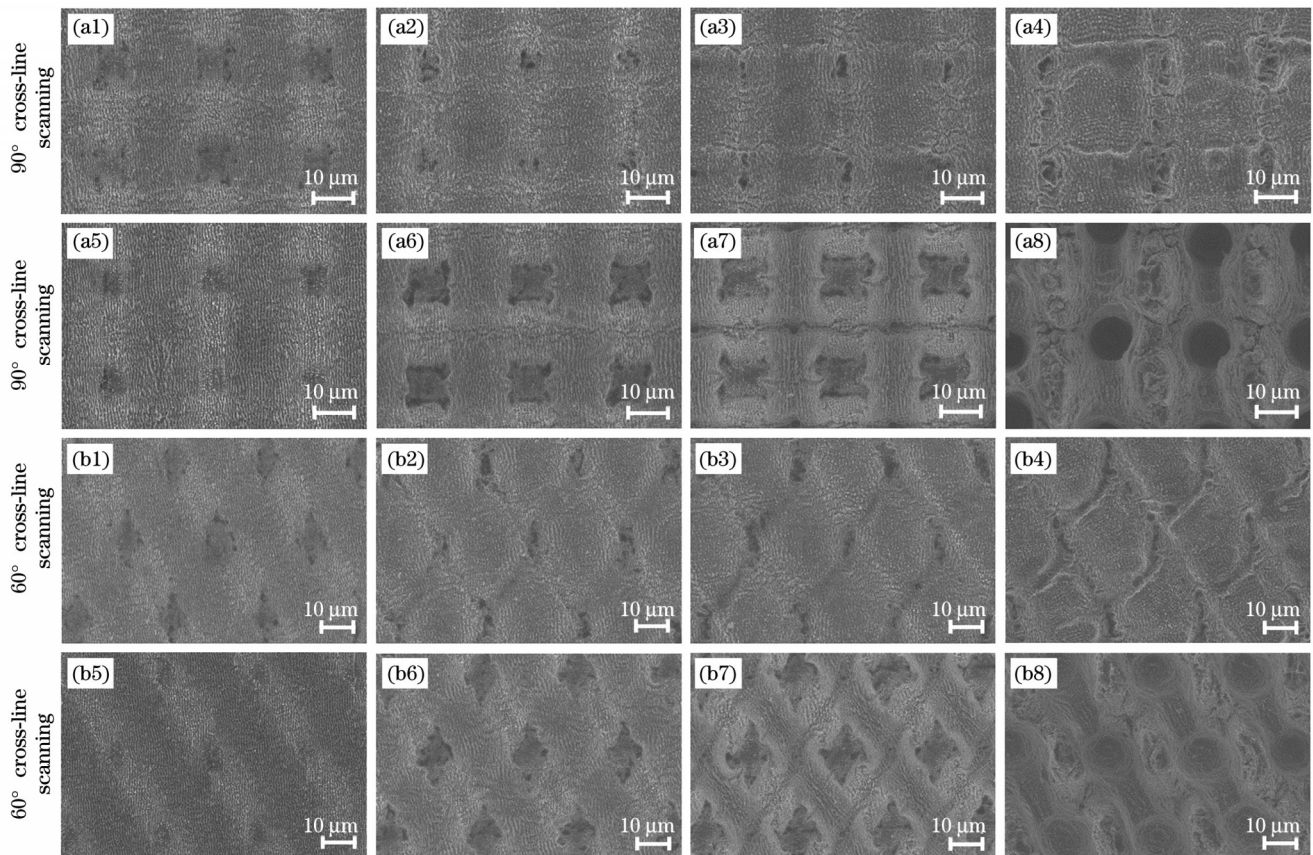


图 3 不同激光能量密度和扫描次数下 90° 和 60° 交叉线扫描获得的 Ti6Al4V 表面 SEM 图像。(a1)(b1) $F=0.20 \text{ J/cm}^2, N=10$; (a2)(b2) $F=0.90 \text{ J/cm}^2, N=10$; (a3)(b3) $F=2.31 \text{ J/cm}^2, N=10$; (a4)(b4) $F=5.51 \text{ J/cm}^2, N=10$; (a5)(b5) $F=0.20 \text{ J/cm}^2, N=5$; (a6)(b6) $F=0.20 \text{ J/cm}^2, N=25$; (a7)(b7) $F=0.20 \text{ J/cm}^2, N=50$; (a8)(b8) $F=2.31 \text{ J/cm}^2, N=50$

Fig. 3 SEM images of Ti6Al4V surfaces obtained by 90° and 60° cross-line scanning under different F and N . (a1)(b1) $F=0.20 \text{ J/cm}^2, N=10$; (a2)(b2) $F=0.90 \text{ J/cm}^2, N=10$; (a3)(b3) $F=2.31 \text{ J/cm}^2, N=10$; (a4)(b4) $F=5.51 \text{ J/cm}^2, N=10$; (a5)(b5) $F=0.20 \text{ J/cm}^2, N=5$; (a6)(b6) $F=0.20 \text{ J/cm}^2, N=25$; (a7)(b7) $F=0.20 \text{ J/cm}^2, N=50$; (a8)(b8) $F=2.31 \text{ J/cm}^2, N=50$

最后,当激光的能量密度 F 和扫描次数 N 分别达到 2.31 J/cm^2 和 50 次时,如图 3(a8)、(b8)所示,激光交叉线扫描重叠区域由于加倍的脉冲作用,出现了大量微孔。此外,在能量密度和扫描次数的共同增幅下,钛合金表面发生了强烈的烧蚀过程和马兰戈尼对流效应^[27],超高的加热速率导致材料表面迅速升温,熔体以液滴和蒸汽的混合物形式爆炸性地无序流出。最后,

较高的扫描次数提供了足够的冷凝时间,相邻扫描路径上流出的熔体通过堆叠,在表面上形成了无规则的微凸起结构。

通过共聚焦显微镜获得了表面结构的截面轮廓与尺寸参数。图 4 显示了在 $N=10$ 的条件下,激光能量密度 F 为 $0.20, 0.90, 2.31, 5.51 \text{ J/cm}^2$ 时两种扫描方式所织构的截面轮廓分布。当激光能量密度 F 为 0.20 J/cm^2

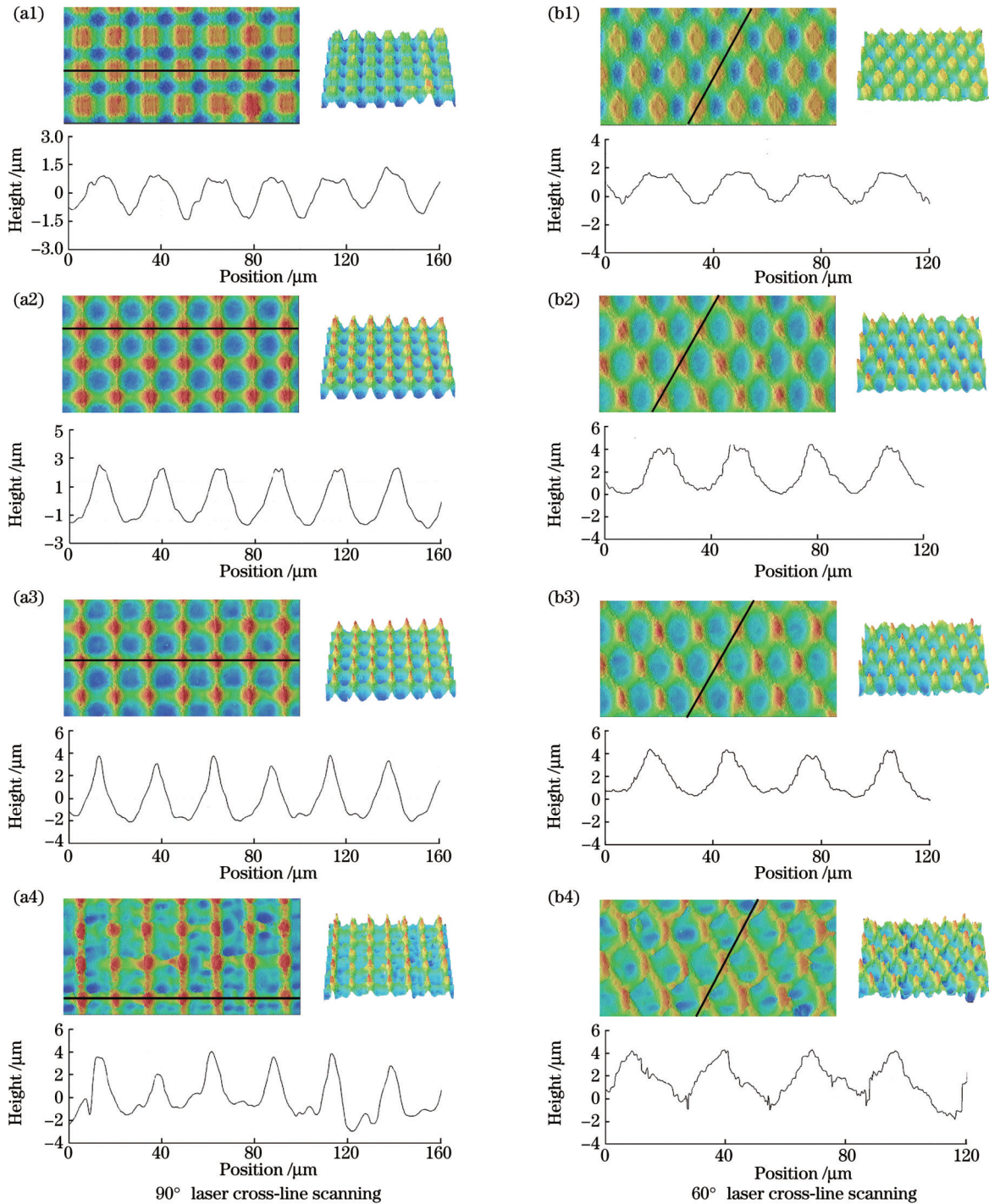


图 4 $N=10$ 时不同能量密度下平行于扫描路径方向的微结构截面轮廓。(a1)(b1) $F=0.20 \text{ J/cm}^2$; (a2)(b2) $F=0.90 \text{ J/cm}^2$; (a3)(b3) $F=2.31 \text{ J/cm}^2$; (a4)(b4) $F=5.51 \text{ J/cm}^2$
 Fig. 4 Cross-sectional profiles of microstructures parallel to scan path direction under different F when $N=10$. (a1)(b1) $F=0.20 \text{ J/cm}^2$; (a2)(b2) $F=0.90 \text{ J/cm}^2$; (a3)(b3) $F=2.31 \text{ J/cm}^2$; (a4)(b4) $F=5.51 \text{ J/cm}^2$

时,由于高斯光束的中心强度相对较弱,因此激光烧蚀去除的材料较少,图4(a1)、(b1)中的表面地势相对平坦;而随着能量密度的增加,材料的烧蚀程度加剧,微结构单元的曲率增大,表面的地势起伏变得更加明显,如图4(a2)、(b2)所示,这也与SEM测量结果中的微结构顶部凸起的现象吻合。当能量密度 F 达到 5.51 J/cm^2 时,如图4(a4)、(b4)所示,由于表面熔体流动不一致,因此微结构的均匀性受到破坏。

详细的表面结构尺寸随激光能量密度的变化如图5所示。采用两种激光扫描方式在相同的激光参数下加工得到的结构尺寸基本相同。表面粗糙度 S_a 和微结构高度在初始的能量密度范围内几乎呈线性增加,但当激光能量密度增幅到 2.31 J/cm^2 时,两者不再随能量密度继续增加,而是趋于饱和。对于这一实验

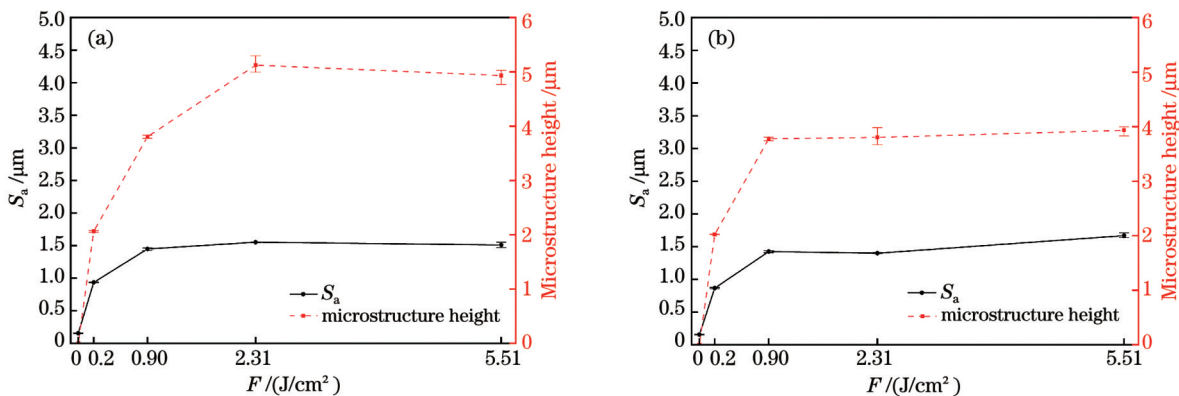


图5 $N=10$ 时采用两种扫描方式在不同能量密度下获得的样品表面粗糙度和微结构高度。(a)90°激光交叉线扫描;(b)60°激光交叉线扫描

Fig. 5 S_a and microstructure heights of samples obtained by two laser scanning methods under different F when $N=10$. (a) 90° laser cross-line scanning; (b) 60° laser cross-line scanning

图6描述的是在激光能量密度 F 为 0.20 J/cm^2 的条件下,扫描次数 N 为5、10、25、50时两种扫描方式所织构的截面轮廓分布。当扫描次数 N 为5时,表面微结构的截面轮廓存在不均匀性,如图6(a1)、(b1)所示;而当扫描次数 N 为25时,表面微结构的截面轮廓基本形成,如图6(a3)、(b3)所示。实际上,在低能量密度下扫描次数的增加仅会导致表面织构的整体形貌发生轻微变化。因为每次激光循环扫描后材料表面上的能量沉积分布保持一致,并且每次激光扫描都会去除一定深度的材料,随着扫描次数的增加,激光通过烧蚀去除的材料增多,导致扫描路径上形成的微沟槽深度增加。同时,由于实验中使用的高斯光束中心强度高于边缘强度,因此激光扫描路径中心处的材料去除率高于边缘,进而形成了微结构倾斜侧壁。当扫描次数达到一定水平时,表面微结构将表现出良好的均匀性和直线度。

织构后的表面粗糙度 S_a 和微结构高度随激光扫描次数 N 的变化如图7所示。未织构钛合金的表面粗糙度 S_a 为 $(0.16 \pm 0.01)\mu\text{m}$,随着扫描次数的增加,表面粗糙度 S_a 和微结构高度呈现持续增加的趋势。这

现象,可以利用等离子体对脉冲激光能量沉积的影响规律进行分析。当飞秒脉冲激光与材料表面相互作用时,材料中的自由电子通过逆韧致辐射机制^[28]吸收入射光子的能量,并在飞秒尺度上与其他电子碰撞而热化。尽管单个飞秒脉冲时间不足以使晶格被加热,多个脉冲沉积后能量还是能够通过电子-声子耦合以热扩散的形式传递给晶格。高温下,束缚态的电子从原子中剥离,产生高温高压的等离子体,并在库伦斥力下迅速脱离材料表面^[29]。同时,高能量密度下超高的加热速率使得材料表面温度迅速升至材料的沸点,过热的液相与大量的蒸汽混合后在高压下迅速膨胀,导致表面发生相爆炸。在高能量密度下,当等离子体密度累积超过临界值时,将会出现高度吸收^[30],从而引起后续激光脉冲能量沉积效率的下降。

是由于随着扫描次数的增加,材料去除量增多,进而微结构顶部重铸层累积所产生的高度发生变化,并最终影响织构样品表面的粗糙度 S_a 。

表面润湿性描述的是液体在固体表面上扩散或黏附而不形成液滴的趋势,通常采用固液相分界线与液滴边缘轮廓切线之间的接触角来表征^[31]。图8(a)、(b)分别显示了在不同的激光能量密度和扫描次数下采用两种扫描方式织构得到的样品表面的接触角测量结果,其中LST表示激光表面织构。未进行激光织构的钛合金表面的左和右接触角分别为 $65.33^\circ \pm 5.98^\circ$ 和 $64.63^\circ \pm 4.40^\circ$ 。经过飞秒激光织构后,液滴在钛合金表面呈现出了不同程度的浸润现象,其与所使用的激光加工参数密切相关。表面的接触角随激光能量密度的增加而减小;而扫描次数的增加对润湿性的影响并不显著,织构后的表面接触角与未织构表面相比略有下降。然而,当激光能量密度和扫描次数共同增加时,钛合金表面的润湿行为发生显著变化,如图8(c)所示,液滴在接触表面后迅速铺展开,3 s后接触角变为 0° 。

飞秒激光织构处理引起钛合金表面亲水性增强的

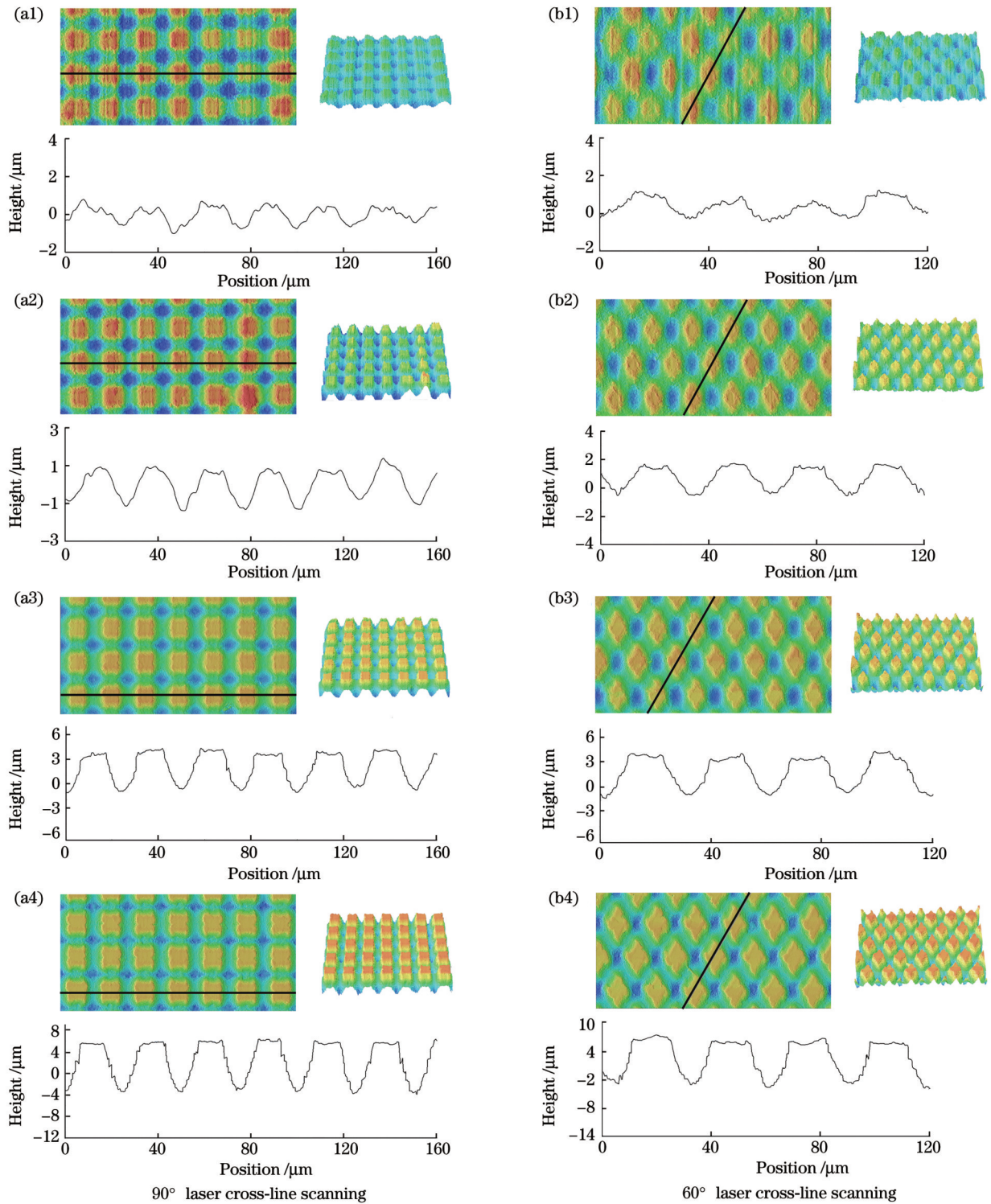


图 6 $F=0.20 \text{ J/cm}^2$ 时不同扫描次数下平行于扫描路径方向的微结构截面轮廓。(a1)(b1) $N=5$; (a2)(b2) $N=10$; (a3)(b3) $N=25$; (a4)(b4) $N=50$
 Fig. 6 Cross-sectional profiles of microstructures parallel to scan path direction under different N when $F=0.20 \text{ J/cm}^2$. (a1)(b1) $N=5$; (a2)(b2) $N=10$; (a3)(b3) $N=25$; (a4)(b4) $N=50$

原因一方面来自表面结构的塑造,织构后钛合金表面结构形貌的改变导致了其与液滴的实际接触面积增大。根据 Wenzel 模型^[32]可知,本征亲水材料由于固相与液相接触面积扩展而会变得更加亲水。然而,仅依赖结构几何参数的变化来解释钛合金表面亲水性增强并不完善。特定的激光加工参数会使表面润湿性能产

生显著变化,在图 8(a)或图 8(b)任意的扫描路径策略中,激光能量密度增加导致表面接触角下降的趋势比扫描次数增加导致接触角下降的趋势更为明显,尽管通过之前的讨论已经证实了增加激光扫描次数使得织构后的表面更加粗糙。除表面结构形貌外,激光织构钛合金引起的表面化学成分变化对润湿行为产生了影响。

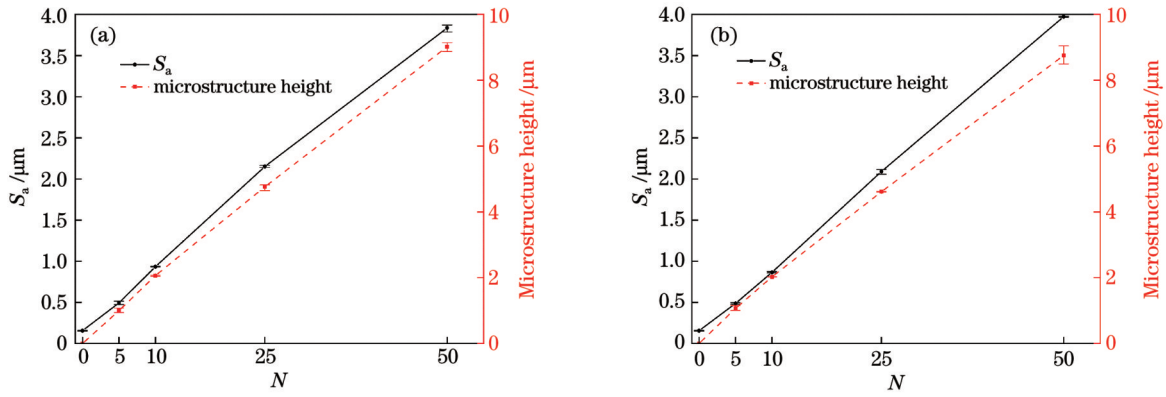


图 7 $F=0.20 \text{ J/cm}^2$ 时采用两种扫描方式在不同扫描次数下获得的样品表面粗糙度和微结构高度。(a)90°激光交叉线扫描;(b)60°激光交叉线扫描

Fig. 7 S_a and microstructure heights of samples obtained by two laser scanning methods under different N when $F=0.20 \text{ J/cm}^2$. (a) 90° laser cross-line scanning; (b) 60° laser cross-line scanning

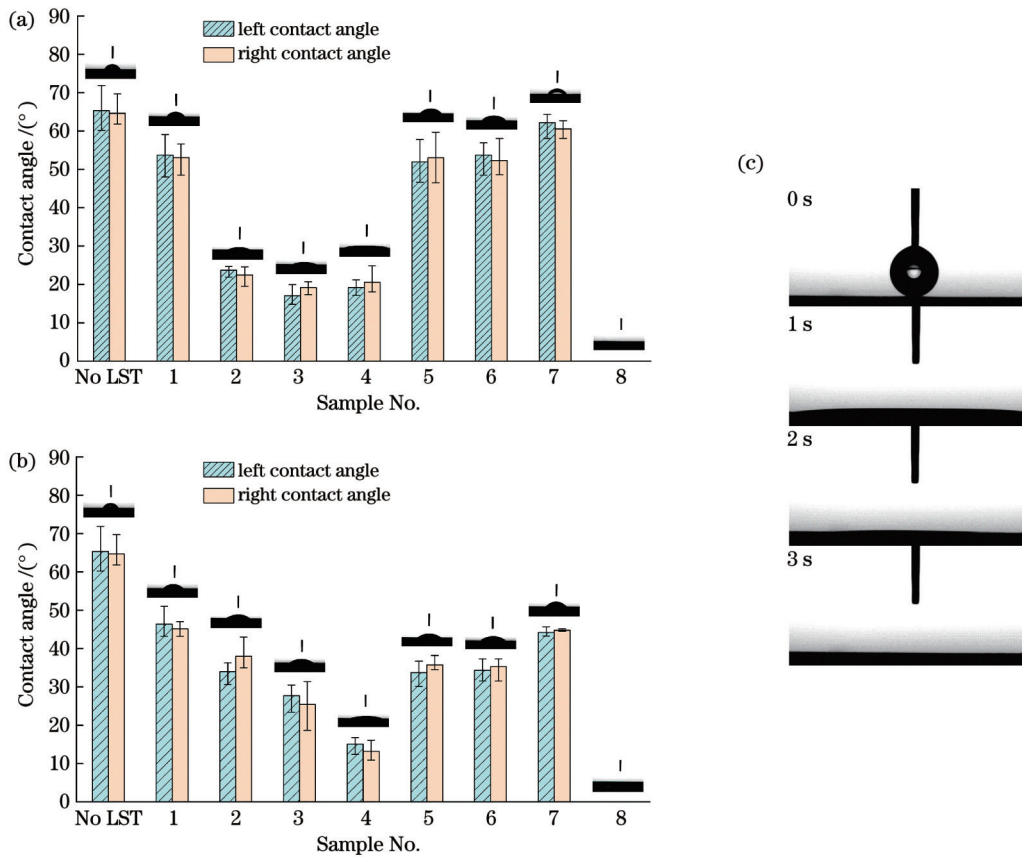


图 8 不同激光能量密度和扫描次数下采用两种扫描方式获得的样品表面接触角。(a)90°激光交叉线扫描;(b)60°激光交叉线扫描;(c)90°激光交叉线扫描方式下激光能量密度为 2.31 J/cm^2 、扫描次数为 50 时表面接触角随时间的变化

Fig. 8 Contact angles of sample surfaces obtained by two laser scanning methods under different N and F . (a) 90° laser cross-line scanning; (b) 60° laser cross-line scanning; (c) contact angle of surface versus time under 90° laser cross-line scanning when $F=2.31 \text{ J/cm}^2$ and $N=50$

为了解不同飞秒激光参数下织构引起的表面化学成分变化以及由此产生的润湿行为,采用90°激光交叉扫描方式制备了四组样品并进行了X射线光电子能谱(XPS)测量。图9为未经激光织构的表面与采用90°激光交叉线扫描方式在不同能量密度和扫描次数下获得的表面XPS图,其中括号里的百分数表示原子数分数。可以看出:各样品表面主要由O、Ti、C、Al和少量的N

元素组成。由于在大气环境中碳通常以有机化合物的形式吸附在材料表面,未经激光织构的样品表面不可避免地检测到了碳元素,但在飞秒激光影响下织构后的钛合金表面的碳元素含量出现下降。此外,与未经激光织构的样品表面相比,激光织构表面的氧元素含量显著增加,而由于金属钛的烧蚀阈值低于铝,因此激光织构表面的钛元素含量下降,铝元素含量相对增加。

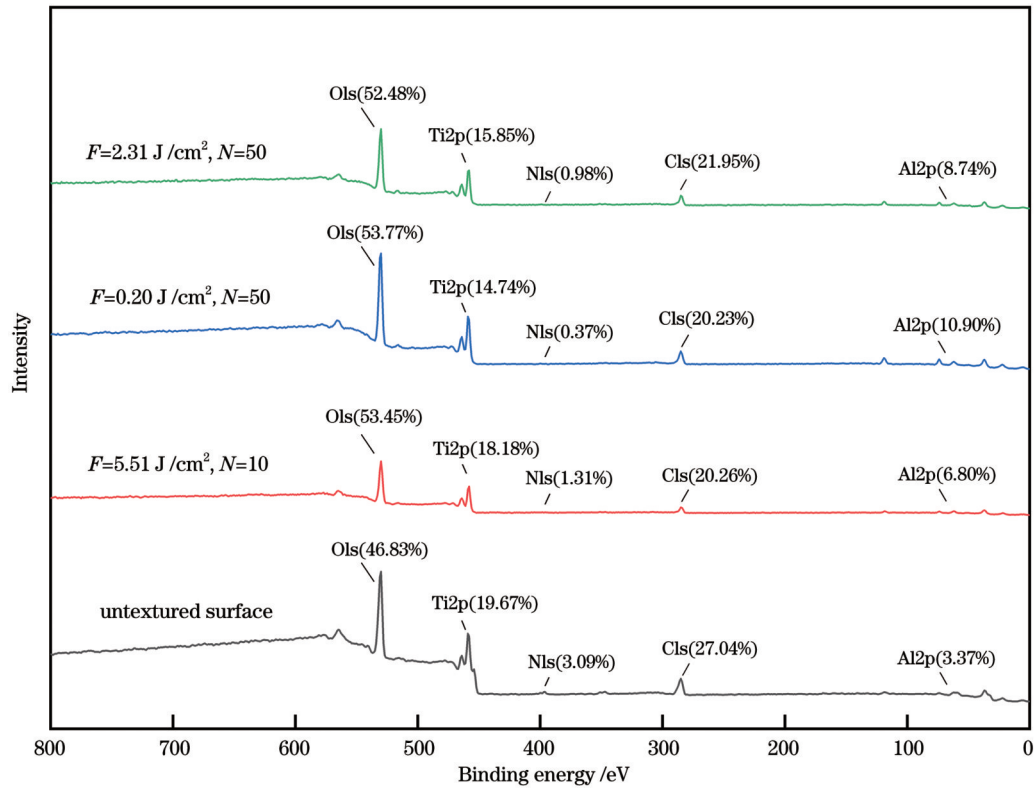


图 9 未经激光织构的表面与采用 90° 激光交叉线扫描方式在不同能量密度和扫描次数下获得的表面 XPS 图
 Fig. 9 XPS diagram of surfaces obtained without laser texture and with 90° laser cross-line scanning under different F and N

进一步的元素基团组成分析能够更好地揭示飞秒激光织构钛合金表面引起的化学组分变化。图 10 为

图 9 中四组样品表面 Ti2p 分峰的拟合结果, Ti2p 由于自旋轨道分裂而出现了双峰。可以看出, 未经激光织

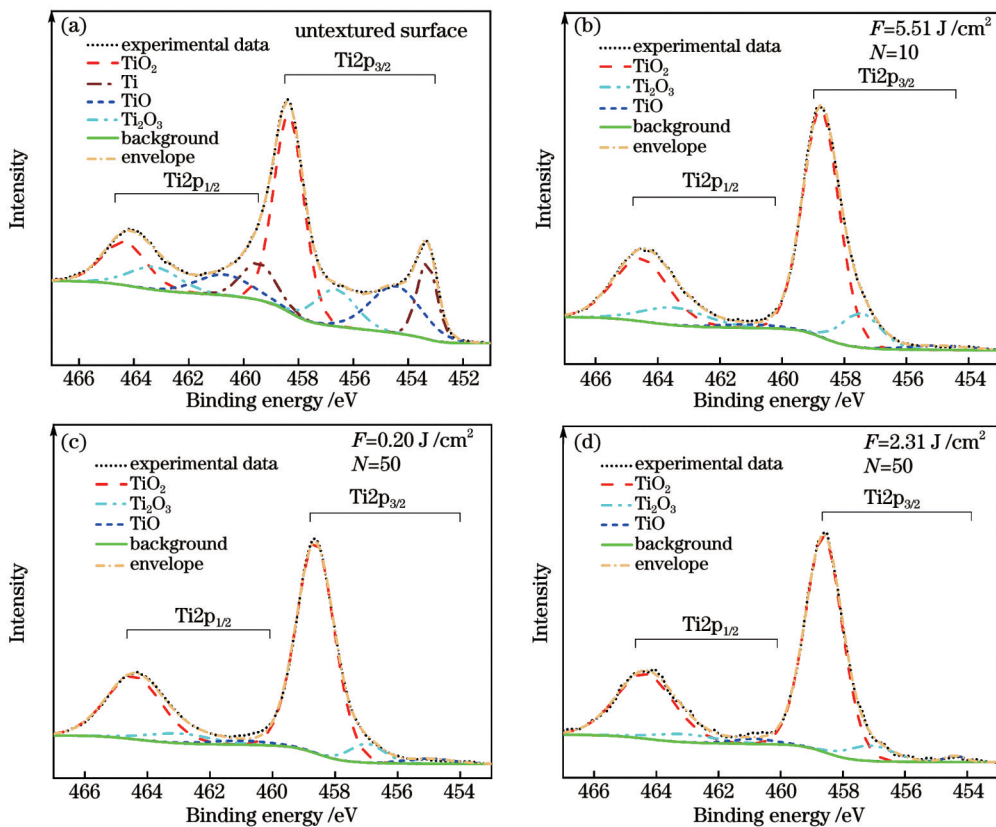


图 10 未经激光织构的表面与采用 90° 激光交叉线扫描方式在不同能量密度和扫描次数下获得的表面 Ti2p 的精细谱图
 Fig. 10 Ti2p fine spectra of surfaces obtained without laser texture and with 90° laser cross-line scanning under different F and N

构表面的 Ti2p 峰包含了 TiO₂、Ti₂O₃、TiO 和 Ti 的四种双峰信号,而其余三种激光织构表面的 Ti2p 峰均没有 Ti 的双峰信号。结合 XPS 图中氧元素的含量变化,发现飞秒激光织构钛合金表面时发生了氧化反应,金属钛和铝与空气中的氧元素结合,在表面上生成了大量的金属氧化物,这一过程与飞秒激光参数的选取有关。较高的激光能量密度或扫描次数促进了金属钛转化为高价钛的金属氧化物,这些金属氧化物能够提供大量的不饱和金属和氧原子作为路易斯酸碱位点^[33],快速吸附空气中的水分子,导致羟基化反应^[34],从而导致钛合金表面的亲水性增强。如图 10 所示,当激光的能量密度和扫描次数分别达到 2.31 J/cm²和 50 时,表面钛元素基团主要以 Ti⁴⁺的氧化物形式存在。此时,结构形貌相对粗糙,并伴随有表面氧化物的富集,这进一步促进了液滴的浸润。

4 结 论

通过飞秒激光辐照 Ti6Al4V 表面可以很好地构建具有不同表面形貌和尺寸的有序结构。尽管增加激光能量密度和扫描次数都有助于增大钛合金表面粗糙度,但在烧蚀方面存在明显差异。激光能量密度的大小直接影响了材料表面的烧蚀程度,织构后的表面粗糙度在高能量密度下由于等离子体屏蔽作用而趋于饱和;扫描次数决定了微结构的高度和微沟槽的深度,扫描次数越高,表面粗糙度越大。合适的激光能量密度和扫描次数有利于在钛合金表面上形成规则的微结构分布。此外,飞秒激光加工过程增强了钛合金表面的亲水性,在不同的激光参数下织构获得的表面亲水程度不一。特别是当激光能量密度为 2.31 J/cm²、扫描次数为 50 时,实现了液滴接触后迅速扩散的超亲水表面。虽然激光能量密度和扫描次数可通过改变表面结构形貌和特征尺寸来影响表面的润湿性,但进一步的分析结果表明,钛合金表面润湿行为的改变并不完全依赖于结构几何参数,激光烧蚀引起的表面化学成分变化也是影响表面润湿性的重要因素。

参 考 文 献

- [1] Dileep M, Majumdar J D. Short and ultrashort laser surface processing of Alpha + Beta titanium alloy (Ti6Al4V): present status[J]. Transactions of the Indian National Academy of Engineering, 2022, 7(3): 851-871.
- [2] Najeeb S, Mali M, Syed A U Y, et al. Dental implants materials and surface treatments[M] // Advanced dental biomaterials. Amsterdam: Elsevier, 2019: 581-598.
- [3] Curran J M, Chen R, Hunt J A. Controlling the phenotype and function of mesenchymal stem cells *in vitro* by adhesion to silane-modified clean glass surfaces[J]. Biomaterials, 2005, 26(34): 7057-7067.
- [4] Gnilitzkiy I, Pogorielov M, Viter R, et al. Cell and tissue response to nanotextured Ti6Al4V and Zr implants using high-speed femtosecond laser-induced periodic surface structures[J]. Nanomedicine: Nanotechnology, Biology, and Medicine, 2019, 21: 102036.
- [5] Cruz M B, Silva N, Marques J F, et al. Biomimetic implant surfaces and their role in biological integration—a concise review[J]. Biomimetics, 2022, 7(2): 74.
- [6] Liu Y, Liu J D, Li S Y, et al. One-step method for fabrication of biomimetic superhydrophobic surface on aluminum alloy[J]. Colloids and Surfaces A: Physicochemical and Engineering Aspects, 2015, 466: 125-131.
- [7] Xie L K, Tang Z G, Jiang L, et al. Creation of superhydrophobic wood surfaces by plasma etching and thin-film deposition[J]. Surface and Coatings Technology, 2015, 281: 125-132.
- [8] Qian B T, Shen Z Q. Fabrication of superhydrophobic surfaces by dislocation-selective chemical etching on aluminum, copper, and zinc substrates[J]. Langmuir, 2005, 21(20): 9007-9009.
- [9] He W Y, Yao P, Chu D K, et al. Controllable hydrophilic titanium surface with micro-protrusion or micro-groove processed by femtosecond laser direct writing[J]. Optics & Laser Technology, 2022, 152: 108082.
- [10] Ahmed K, Grambow C, Kietzig A M. Fabrication of micro/nano structures on metals by femtosecond laser micromachining[J]. Micromachines, 2014, 5(4): 1219-1253.
- [11] Li C, Zhang H, Cheng G, et al. Initial cumulative effects in femtosecond pulsed laser-induced periodic surface structures on bulk metallic glasses[J]. Journal of Laser Micro, 2016, 11(3): 357-365.
- [12] 王翼猛, 管迎春. 飞秒激光诱导医用金属材料表面功能微纳结构的研究进展[J]. 中国激光, 2022, 49(10): 1002601.
Wang Y M, Guan Y C. Progress in preparation of medical functional surfaces by femtosecond laser-induced micro/nanostructures[J]. Chinese Journal of Lasers, 2022, 49(10): 1002601.
- [13] Cunha A, Serro A P, Oliveira V, et al. Wetting behaviour of femtosecond laser textured Ti-6Al-4V surfaces[J]. Applied Surface Science, 2013, 265: 688-696.
- [14] Huerta-Murillo D, García-Girón A, Romano J M, et al. Wettability modification of laser-fabricated hierarchical surface structures in Ti-6Al-4V titanium alloy[J]. Applied Surface Science, 2019, 463: 838-846.
- [15] Schnell G, Staehle S, Duenow U, et al. Femtosecond laser nano/micro textured Ti6Al4V surfaces—effect on wetting and MG-63 cell adhesion[J]. Materials, 2019, 12(13): 2210.
- [16] Pallarés-Aldeiturriaga D, Papa S, Abou Khalil A, et al. Influence of multi-wavelength ultrafast laser texturing and autoclave sterilization on titanium alloy-based surface wettability[J]. Applied Physics A, 2022, 128(10): 894.
- [17] Vorobyev A Y, Guo C L. Femtosecond laser structuring of titanium implants[J]. Applied Surface Science, 2007, 253(17): 7272-7280.
- [18] Dumas V, Rattner A, Vico L, et al. Multiscale grooved titanium processed with femtosecond laser influences mesenchymal stem cell morphology, adhesion, and matrix organization[J]. Journal of Biomedical Materials Research. Part A, 2012, 100(11): 3108-3116.
- [19] Cunha A, Zouani O F, Plawinski L, et al. Human mesenchymal stem cell behavior on femtosecond laser-textured Ti-6Al-4V surfaces[J]. Nanomedicine, 2015, 10(5): 725-739.
- [20] Dumas V, Guignandon A, Vico L, et al. Femtosecond laser nano/micro patterning of titanium influences mesenchymal stem cell adhesion and commitment[J]. Biomedical Materials, 2015, 10(5): 055002.
- [21] Raimbault O, Benayoun S, Anselme K, et al. The effects of femtosecond laser-textured Ti-6Al-4V on wettability and cell response[J]. Materials Science and Engineering: C, 2016, 69: 311-320.
- [22] Chen P, Aso T, Sasaki R, et al. Adhesion and differentiation behaviors of mesenchymal stem cells on titanium with micrometer and nanometer-scale grid patterns produced by femtosecond laser irradiation[J]. Journal of Biomedical Materials Research. Part A, 2018, 106(10): 2735-2743.

- [23] Li H Y, Wang X, Zhang J J, et al. Experimental investigation of laser surface texturing and related biocompatibility of pure titanium [J]. *The International Journal of Advanced Manufacturing Technology*, 2022, 119(9): 5993-6005.
- [24] Maharjan N, Zhou W, Zhou Y, et al. Ablation morphology and ablation threshold of Ti-6Al-4V alloy during femtosecond laser processing[J]. *Applied Physics A*, 2018, 124(8): 519.
- [25] Huang M, Zhao F L, Cheng Y, et al. Origin of laser-induced near-subwavelength ripples: interference between surface plasmons and incident laser[J]. *ACS Nano*, 2009, 3(12): 4062-4070.
- [26] Wang Y F, Yu Z, Li K M, et al. Study on the effect of surface characteristics of short-pulse laser patterned titanium alloy on cell proliferation and osteogenic differentiation[J]. *Materials Science and Engineering: C*, 2021, 128: 112349.
- [27] 何婉盈, 姚鹏, 褚东凯, 等. 钛表面微凹凸结构的激光加工及其细胞黏附研究[J]. *中国激光*, 2022, 49(10): 1002605.
He W Y, Yao P, Chu D K, et al. Fabrication and cell-adhesion evaluation of laser-ablated microprotrusion or microgroove on titanium[J]. *Chinese Journal of Lasers*, 2022, 49(10): 1002605.
- [28] Chichkov B N, Momma C, Nolte S, et al. Femtosecond, picosecond and nanosecond laser ablation of solids[J]. *Applied Physics A*, 1996, 63(2): 109-115.
- [29] Zheng B X, Jiang G D, Wang W J, et al. Ablation experiment and threshold calculation of titanium alloy irradiated by ultra-fast pulse laser[J]. *AIP Advances*, 2014, 4(3): 031310.
- [30] Miotello A, Kelly R. Laser-induced phase explosion: new physical problems when a condensed phase approaches the thermodynamic critical temperature[J]. *Applied Physics A*, 1999, 69(1): S67-S73.
- [31] 白雪, 陈烽. 飞秒激光制备超疏水表面的研究进展[J]. *光学学报*, 2021, 41(1): 0114003.
Bai X, Chen F. Recent advances in femtosecond laser-induced superhydrophobic surfaces[J]. *Acta Optica Sinica*, 2021, 41(1): 0114003.
- [32] Wenzel R N. Resistance of solid surfaces to wetting by water[J]. *Industrial & Engineering Chemistry*, 1936, 28(8): 988-994.
- [33] Hass K C, Schneider W F, Curioni A, et al. The chemistry of water on alumina surfaces: reaction dynamics from first principles [J]. *Science*, 1998, 282(5387): 265-268.
- [34] Azimi G, Dhiman R, Kwon H M, et al. Hydrophobicity of rare-earth oxide ceramics[J]. *Nature Materials*, 2013, 12(4): 315-320.

Morphology and Wettability of Titanium Alloy Surface Textured by Femtosecond Laser

Xiao Pulu^{1,2}, Chen Guanhua^{1,2}, Chen Yu⁵, Zhang Xiang^{1,2,3,4}, Yuan Xiao^{1,2,3,4*}

¹*School of Optoelectronic Science and Engineering, Soochow University, Suzhou 215006, Jiangsu, China;*

²*Collaborative Innovation Center of Suzhou Nano Science and Technology, Soochow University, Suzhou 215006, Jiangsu, China;*

³*Key Lab of Advanced Optical Manufacturing Technologies of Jiangsu Province, Suzhou 215006, Jiangsu, China;*

⁴*Key Lab of Modern Optical Technologies of Education Ministry of China, Soochow University, Suzhou 215006, Jiangsu, China;*

⁵*Amplitude Shanghai Laser Technology Co., Ltd., Suzhou 215123, Jiangsu, China*

Abstract

Objective In recent decades, the global market demand for dental and orthopedic implants has grown steadily owing to an aging population, an increase in bad habits, and frequent accidents. Titanium alloys have a low specific gravity, high corrosion resistance, better compressive strength, and fracture toughness than other implant materials and are currently widely used in biomedical implant engineering. However, owing to the biological inertia of titanium alloys, long-term implantation may induce inflammation around the implant and affect its lifespan. To realize a tight connection between the implant and the surrounding tissue of the human body and form a stable osseointegration interface, the modification of the implant surface is very important. Among these surface properties, wettability mainly affects the type, quantity, and conformation of proteins deposited on the implant surface, and subsequently affects the cell response at the material interface. With deeper research on the surface modification of laser-irradiated materials, the coupling relationship between various surface properties after modification becomes complicated when considering the functional effect of hydrophilicity alone. However, the differences in the surface morphology make the relationship between wettability and cell biological behavior inconclusive. Therefore, it is necessary to systematically evaluate the wettability of surfaces with different structural features after femtosecond-laser texturing. The scanning path strategy and structural changes caused by laser parameters proposed in this study provide ideas for the design and construction of biomedical implant surface structures.

Methods Ti6Al4V sheets with a thickness of 0.5 mm are prepared for the experimental study. Before processing, the samples are polished using an abrasive wheel, followed by ultrasonic cleaning in deionized water, acetone, and absolute ethanol for 15 min. Surface texturing is performed using a ytterbium fiber laser with a central wavelength of 1030 nm and a pulse duration of 300 fs. Sixteen samples are fabricated using two scanning path strategies to determine the effects of laser parameters on the surface structure and wettability. A scanning electron microscope (SEM) is used to observe the structural morphology of the processed sample surfaces. The cross-sectional morphology and surface roughness S_a of the samples are characterized using a confocal microscope. To evaluate the wetting properties, the static contact angles of the sample surfaces are measured using a video optical contact angle meter. The X-ray photoelectron spectroscopy (XPS) is used to detect the chemical compositions of the sample surfaces before and after femtosecond laser texturing.

Results and Discussions In this study, the surface of titanium alloy is textured by changing the laser energy density and number of scans. With increasing laser energy density, the top of the microstructure gradually bulges, and the laser induced periodic surface structure (LIPSS) bifurcates and produces a large number of surface nanoparticles. When the number of scans increases, a thick recast layer appears on the edge of the microstructure, whereas the LIPSS structure does not disappear because of the low energy density (Fig. 3). The surface topography becomes more undulating as the laser energy density increases, which is consistent with the SEM image results (Fig. 4). The surface roughness S_a and microstructure height do not increase linearly with the energy density but tend to saturate (Fig. 5). Increasing the number of scans results in slight changes in the overall surface topography (Fig. 6). With an increase in the number of scans, the surface roughness and microstructure height exhibit continuously increasing trends (Fig. 7). After femtosecond laser texturing, the hydrophilicity of all surfaces improves, and the contact angle decreases with increasing energy density. The effect of the number of scans on the surface wettability is not significant at low energy density values, and the contact angle decreases slightly compared to that of the untextured samples. However, when both the laser energy density and number of scans are increased, the wetting behavior of the material surface changes drastically, and a superhydrophilic surface that is rapidly wetted by the droplet within 3 s is observed (Fig. 8). The XPS results show that the femtosecond-laser texturing changes the chemical composition of the titanium alloy surface. The carbon content decreases and the oxygen content increases significantly (Fig. 9). The further analysis of the Ti2p fine spectra shows that an oxidation reaction occurs when the femtosecond laser textures the surface of the titanium alloy, and a high laser energy density or number of scans promotes the conversion of elemental titanium to high-valence titanium oxide (Fig. 10).

Conclusions Femtosecond laser irradiation of a Ti6Al4V surface can be used to effectively construct designed structures with different morphological and dimensional characteristics. Although both the laser energy density and number of scans contribute to an increase in the surface roughness of titanium alloys, there is a fundamental difference in terms of ablation. The energy density directly affects the degree of laser ablation on the surface, and the surface roughness is saturated by the plasma shielding at high energy density. The number of scans determines the height of the microstructure and the depth of the grooves; the higher the number of scans, the greater the surface roughness. Appropriate energy density values and numbers of scans help maintain a titanium alloy surface with regular microstructural features. Moreover, femtosecond laser processing significantly improves the hydrophilicity of the titanium alloy surface. A superhydrophilic surface with rapid droplet spreading is obtained at the laser energy density of 2.31 J/cm^2 and the number of scans of 50, which may be attributed to the porous morphology with high roughness created by the increase in the laser energy density and number of scans. However, further research shows that the surface hydrophilicity of titanium alloys is not entirely dependent on the surface structural dimensions, and that the surface chemical composition changes caused by laser ablation also mediate the surface wetting process.

Key words laser technique; femtosecond laser; surface texture; titanium alloy; hydrophilicity